PIONEER
ACADEMIC PUBLISHING LIMITED

Journal of Progress in Engineering and Physical Science
ISSN 2709-4006
www.pioneerpublisher.com/jpeps
Volume 3 Number 1 March 2024

# Research on the Performance of 3×7Φ15.2 mm Prestressed Steel Strands and Concrete in Pullout Tests

**Wenhao Zhang[1], Rihua Yang[1] & Wuxiang Zou[1]**

[1] School of Civil Engineering, Hunan City University, Yiyang 413000, China
Correspondence: Wenhao Zhang, School of Civil Engineering, Hunan City University, Yiyang 413000, China.

doi:10.56397/JPEPS.2024.03.08

**Abstract**

In order to study the constitutive model of bond-slip between prestressed steel strands and concrete, pullout tests were designed with 1×7Φ15.2 mm and 3×7Φ15.2 mm concrete specimens. The influence of the number of steel strands on the failure mode, slip characteristics, and concrete strain of pullout specimens was analyzed, and the bond mechanism of 3×7Φ15.2 mm prestressed steel strand bundles was clarified.

**Keywords:** steel strand bundle, pullout test, Bond-slip, prestressed concrete

## 1. Introduction

The effective bond between prestressing tendons and grouting interfaces is the basis for their synergistic work. Currently, scholars at home and abroad (Zhang HY, Kodur V, Wu B, Yan J & Yuan ZS, 2018; Phan TS RP & Tailhan J-L, 2015; Panteki E, Máca P & Häussler-Combe U, 2017) have conducted extensive research on the bond performance between ordinary reinforcement and concrete. It is pointed out that the bond performance of reinforcement is influenced by factors such as reinforcement diameter, shape, concrete strength, cover thickness, and loading rate. Compared with ordinary reinforcement, the unique twisting shape and material differences of prestressing tendons make the bond behavior between them and concrete more complex. Some scholars (Kearsey EP & Joyce A, 2014; Choi YS, Yi S-T, Kim MY, Jung WY & Yang EI, 2014; Fang C, Lundgren K, Chen L & Zhu C, 2004; Bhargava K, Ghosh AK, Mori Y & Ramanujam S, 2008; Bhargava K, Ghosh AK, Mori Y & Ramanujam S, 2007; Wang X & Liu X, 2004; Coronelli D, 2002) have conducted experimental studies on the bond performance of single steel strands and proposed predictive models for the bond performance of single steel strands. The research found that the slip relationship between concrete and steel strands approaches the limit bond force during initial slip, with a distinct yield plateau segment. The bond force between them is affected by concrete strength, steel strand diameter, and concrete cover thickness. Khalaf and Oh (Cherry BW & Price SM, 1980; Schroeder RM & Müller IL, 2003) explored the influence of prestressing tendon diameter and type on its bond performance.

Prestressed strands as a combination of multiple

prestressing tendons have more complex bond behavior. Firstly, the bond between prestressed strands and grouting interfaces will inevitably be affected by the interaction of various tendons, and the degree of influence varies with the number of prestressing tendons, resulting in different bonding strengths of each tendon in the prestressed strand bundle (Zhang B BB, 2004). Secondly, there are differences in the positions, surface conditions, and contact conditions of each tendon in the prestressed strand bundle, resulting in the bond performance having non-uniformity (Zhi Fang KZ & Bing Tu, 2013); moreover, the prestressed strand bundle is not directly in contact with concrete, and its bond performance is also affected by grouting quality and corrugated pipes. Currently, the bonding mechanism between multiple prestressed steel strands in commonly used bridge prestressed steel strand bundles and concrete has not been clearly defined, lacking systematic research.

Therefore, this paper intends to conduct research on the bond performance between multiple prestressed steel strands and concrete, design single-strand and multi-strand prestressed tendon specimens for pullout tests, analyze the influence of the number of prestressing tendons on the failure mode, slip characteristics, and concrete strain of pullout specimens, and clarify the bond mechanism of multi-strand prestressed steel strand bundles.

## 2. Experimental Design

### *2.1 Specimen Design*

Two pullout specimens with a length of 1000mm were designed for this experiment, numbered PLS1-PLS2. PLS1 is a single-strand comparison specimen with a prestressed tendon type of Φ15.2 single-strand 7-wire twisted steel strand; PLS2 has a prestressed tendon type of Φ15.2 three-strand 7-wire twisted steel strand bundle. The cross-sectional dimensions of the pullout specimens are 300 mm × 500 mm. Eight longitudinal main rebars with a diameter of Φ12 mm of HRB400 deformed steel bars were arranged, and the stirrups were Φ8 mm HPB235 round steel bars with a spacing of 100 mm. The steel strands were placed in the center of the specimen, and the detailed dimensions and reinforcement layout of the specimens are shown in Figure 1 and Figure 2.

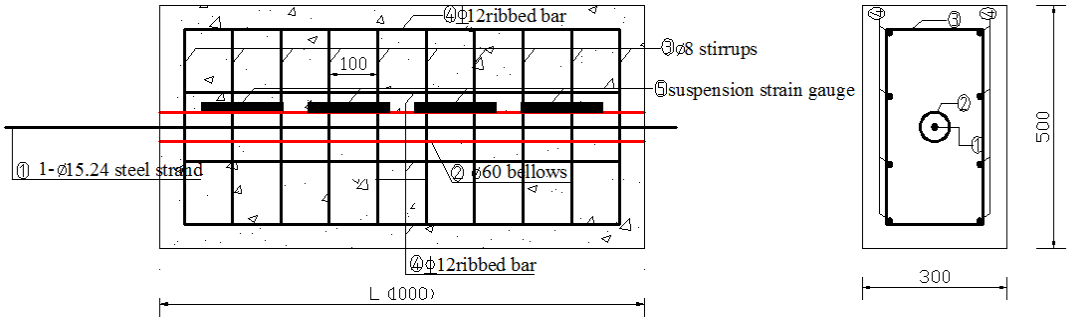


**Figure 1.** Dimension and reinforcement of specimen PLS1

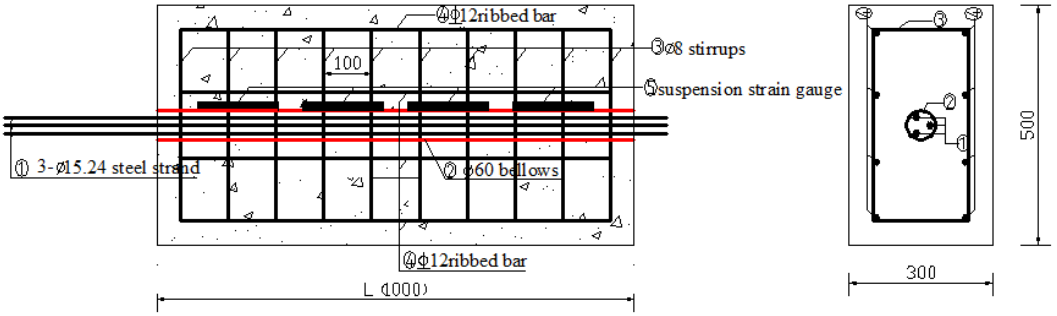


**Figure 2.** Dimension and reinforcement of specimen PLS2

The ordinary reinforcement consisted of a main tensile bar of HRB-grade ribbed steel bar with a diameter of 16 mm, a compressive zone ordinary steel bar of HRB400-grade ribbed steel bar with a

diameter of 10 mm, and stirrups of HPB400-grade round steel bars with a diameter of 8 mm. The prestressed tendon used a diameter of 15.2 mm 1860-grade 7-strand steel strand. The prestressing force of the steel strand was set at 1395 MPa. Two test specimens were cast with the same batch of concrete at once, and the same batch of concrete was used to make cubic standard specimens for curing together with the test specimens. The average compressive strength of concrete at 28 days was 53.5 MPa.

*2.2 Test Equipment and Sensor Arrangement*

According to the test regulations for the grip strength between concrete and steel strands, a pullout device was designed. After the test specimens were completed, a 150-ton range through-core jack was used for tensioning, and a force anchor meter was used to measure the pullout force.

Since the test steel strands were twisted into seven strands and had a twist angle, it was not possible to groove the steel strands or attach strain gauges to monitor the strains of the steel strands. Therefore, by setting spaced strain gauges on the outer wall of the corrugated pipe at a distance of 17.5 cm, the strains of concrete were monitored, and based on this, the strain distribution and real-time bond length of the steel strands were estimated. Strain gauge distribution and pullout test setup are shown in Figure 3.

**Figure 3.** Pullout test setup

Before the formal pullout test of the specimens, the steel strands were pre-tensioned, and the pre-tensioning force was set at 5 kN. After pre-tensioning was completed, the reading of the anchor meter at the loading end and the reading of the dial gauge were zeroed, and then the formal loading program was entered. Load control was carried out in stages, with initial loading every 5 kN, reaching 15 kN, and then increasing by 15 kN per level. The pullout test was immediately stopped if any of the following occurred during the test: the steel strand was pulled out or broken; the slip amount at the loading end was large, and the load could not continue to increase or increased very slowly, indicating bond slip failure.

## 3. Experimental Results and Analysis

*3.1 Failure Mode*

During the test, both PLS1 and PLS2 experienced steel strand breakage, and when the length of both specimens reached 1000 mm, they had sufficient bond length to provide the maximum bond force of the steel strands without exceeding their ultimate tensile strength. For the PLS1 specimen, the slip amount at the free end of the steel strand was close to zero, with almost no slip, and all strands of the steel strand broke almost simultaneously, without concrete splitting failure or complete strand pullout. However, for the PLS2 specimen, the slip amount at the tensioning end of the steel strand increased much faster than for PLS1, and the slip amount at the free end also increased rapidly. Neither specimen showed splitting failure, indicating that they had sufficient cover thickness.

*3.2 Load-Slip Performance*

During the pullout test, it was found that the slip composition of steel strands was not consistent with ordinary deformed steel bars; their slip occurred along the twisted steel strands, similar to the slip of a long helix. The reason for this should be related to the twisting of the steel strands during fabrication, so their slip included both linear slip along the axis of the steel strand and rotation. This demonstrates that twisted steel strands slip in concrete similarly to a helix being screwed into a nut. However, unlike metal nuts with significant ductility, concrete nuts are brittle materials, and the threads are more easily damaged, weakening the rotational restraint effect, which then causes direct pullout slip between the steel strand and concrete. Additionally, as the load increases, after each rotation slip, there is a certain decrease in

loading. Continuing loading causes the still unbroken concrete threads to come into play, and then the load continues to increase, resulting in a serrated shape on the load-slip curve. This serration occurs because the concrete, acting as a nut, is a brittle material, and its threads are easily damaged by the twisted steel wires of the steel strand. The total pullout slip of the steel strand is composed of both linear slip and rotational slip. Linear slip refers to the direct pullout slip of the steel strand along its axis; rotational slip refers to the slip generated by the rotation of the steel strand ends. As a result, the bond action between them gradually weakens after the bond force is completely lost, and the bond force is mainly composed of the frictional force between concrete and steel strands and the interlocking force between the twisted wires in the twisting direction.

Figure 4 presents the load-slip curves at the loading end and free end of PLS1 and PLS2. For the PLS1 specimen, as the pullout force gradually increased, the slip amount increased accordingly. When the pullout force was less than 90 kN, the slip value showed a linear relationship with the pullout force. Afterward, the pullout force and the slip amount at the pullout end showed a nonlinear relationship, with the slip amount increasing significantly faster than the pullout force, and finally, the pullout force increased slightly, but the slip value increased rapidly, leading to steel strand rupture. At the same time, almost no slip amount was measured at the free end throughout the pullout process. Since the steel strands broke during the pullout test, their maximum load corresponds to the ultimate tensile strength of the steel strands. As the bond between concrete and steel strands at the free end had not been broken, the maximum bond force that the specimen could provide was inevitably greater than the ultimate tensile strength of the steel strands.

Additionally, Figure 4 shows that the load-slip curves of single-strand steel strands and three-strand steel strand bundles are not consistent. The PSL2 specimen showed slip at the free end, and serrations appeared at the pullout end, indicating that the effective bond length of PLS2 was significantly greater than that of PLS1. Furthermore, from the load-slip curves of PLS1 and PSL2, the ultimate pullout loads were 262 kN and 776 kN, respectively. These two specimens could provide effective bonding, and the effective bond length was smaller than the designed bond length of the specimen. The reason is that due to the small spacing between multiple steel strands in the steel strand bundle, the cracked areas around each steel strand in the concrete overlap each other, widening the microcracks, and the crack range is significantly greater than that of a single-strand specimen. According to the thick-wall cylinder theory, the cracked concrete in a single bundle with multiple strands cannot provide the wall thickness of a single-strand steel strand, thus unable to provide sufficient constraint force to the steel strand bundle, resulting in reduced mechanical interlocking force and friction force, leading to both reduced bond stiffness and strength compared to a single-strand steel strand specimen, hence requiring a longer bond length.

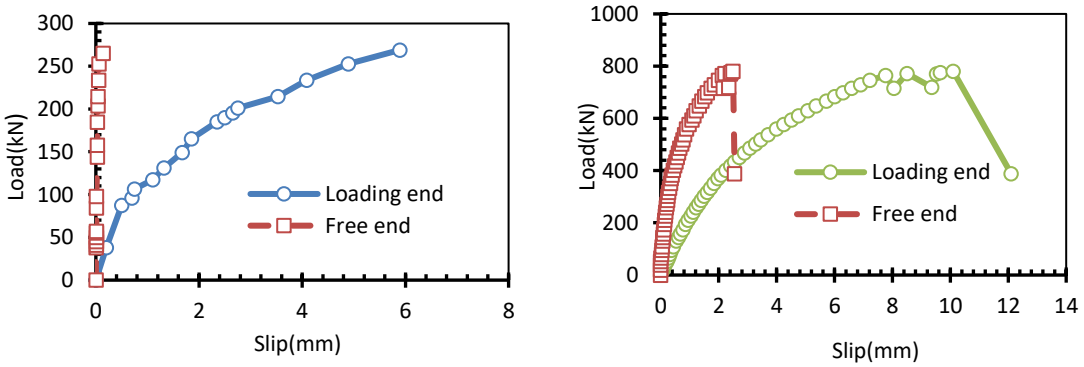


(a) PLS1 (**b**) PLS2

**Figure 4.** Load-slip curves of pullout specimens

*3.3 Concrete Strain Distribution*

By recording the strains of the hanging strain gauges at different pullout loads and connecting them according to their positions, the concrete strains along the pullout end were obtained, as shown in Figure 5. It was assumed during the

experiment that strains were evenly distributed along the entire cross-section, without considering the uneven distribution of strains at the same section affecting the results. From Figure 5, it can be seen that under the action of the pullout force, the concrete strain distribution along the length of the specimen is non-uniform and shows a nonlinear distribution. The slope of the strain lines between adjacent points at the same load and between different points under different pullout forces was not constant. When the pullout force was small, the concrete strain near the tensioning end was significantly higher, and as the pullout force increased, the concrete strain gradually transferred towards the free end, with strain values decreasing from the tensioning end to the free end. There was a significant difference in the initial strain at the free end of the two specimens under the same load. For PLS1, the strain at the free end was zero under the ultimate load, while for PLS2, when the pullout load increased to 200 kN, the concrete even experienced a slight positive strain after initially negative strain, indicating a tiny positive strain. Based on Figure 5, it can be deduced that the effective length under the ultimate load for PLS1 was 88 cm, while for PLS2, it was 100 cm.

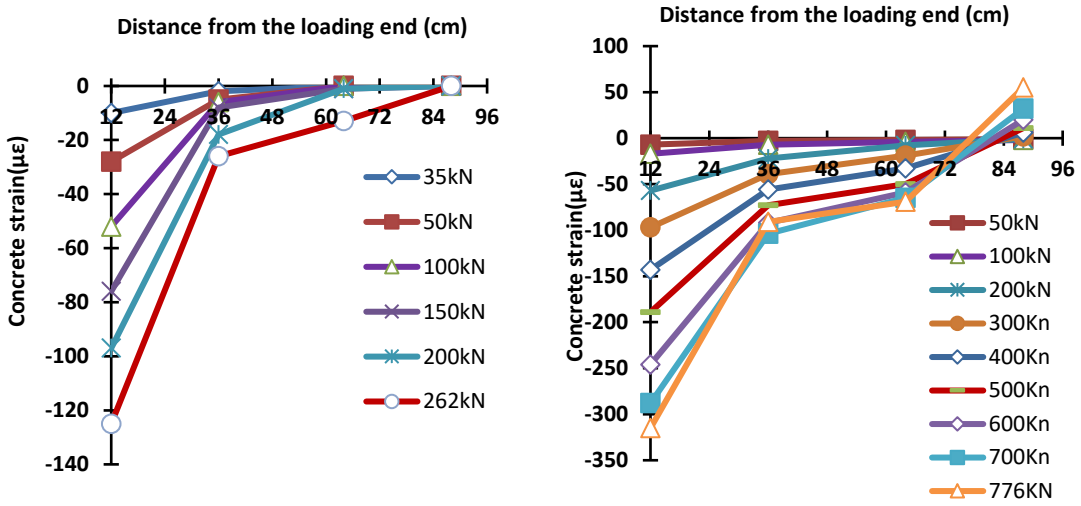


(a) PLS1 (b) PLS2

**Figure 5.** Concrete strain distribution under pullout load

*3.4 Average Bond Stress*

From Figure 5, it can be inferred that the bond stress is not uniformly distributed along the length of the specimen. To discuss the influence of the number of steel strands on the bond stress, it can be assumed that the bond stress is consistent within the bond length range. Therefore, the average bond stress can be calculated using Equation (1):

$$\overline{\tau} = \frac{P}{l_e \sum s} \quad (1)$$

Where: $\overline{\tau}$ is the average bond stress, $P$ is the pullout force, $l_e$ is the effective bond length, and $\sum s$ is the total perimeter of the steel strand.

According to Equation (1), under the ultimate pullout force, the average bond stress of PLS1 is 6.23 MPa, while for PLS2, it is 5.41 MPa, a decrease of 13.2%. It can be seen that compared to the single-strand steel strand specimen, both the stiffness and average bond strength of the three-strand steel strand specimen significantly decreased.

## 4. Conclusion

1) The bond mechanism between steel strands and concrete is similar to that between deformed steel bars and concrete, with bond strength composed of adhesion, friction, and mechanical interlocking forces. However, the difference from deformed steel bars lies in the twisting of steel strands during fabrication, resulting in slip along the steel strand axis as well as rotation.

2) The bond stress of each steel strand in the three-strand prestressed strand bundle is smaller than that of the single-strand steel strand bundle. In this experiment, the average ultimate bond stress of each steel strand in the three-strand steel strand bundle decreased by approximately 13% compared to that of the single-strand steel strand

bundle.

**Fund Project**

This study was supported by the National Undergraduate Training Program for Innovation and Entrepreneurship (S202311527030).

**References**

Bhargava K, Ghosh AK, Mori Y, Ramanujam S. (2007). Corrosion-induced bond strength degradation in reinforced concrete—Analytical and empirical models. *Nuclear Engineering and Design, 237*(11), 1140-57.

Bhargava K, Ghosh AK, Mori Y, Ramanujam S. (2008). Suggested empirical models for corrosion-induced bond degradation in reinforced concrete. *Journal of Structural Engineering, 134*(2), 221-30.

Cherry BW, Price SM. (1980). Pitting,crevice and stress corrosion cracking studies of cold-drawn eutectoid steels. *Corrosion Science, 20*, 1163-84.

Choi YS, Yi S-T, Kim MY, Jung WY, Yang EI. (2014). Effect of corrosion method of the reinforcing bar on bond characteristics in reinforced concrete specimens. *Construction and Building Materials, 54*(0), 180-9.

Coronelli D. (2002). Corrosion cracking and bond strength modeling for corroded bars in reinforced concrete. *ACI Structural Journal, 99*(3), 267-76.

Fang C, Lundgren K, Chen L, Zhu C. (2004). Corrosion influence on bond in reinforced concrete. *Cement and Concrete Research, 34*(11), 2159-67.

Kearsey EP, Joyce A. (2014). Effect of corrosion products on bond strength and flexural behaviour of reinforced concrete slabs. *J S Afr Inst Civ Eng, 56*(2), 21-9.

Panteki E, Máca P, Häussler-Combe U. (2017). Finite element analysis of dynamic concrete-to-rebar bond experiments in the push-in configuration. *International Journal of Impact Engineering, 106*, 155-70.

Phan TS RP, Tailhan J-L. (2015). Numerical modelling of the concrete/rebar bond. *Cement and Concrete Composites, 59*, 9.

Schroeder RM, Müller IL. (2003). Stress corrosion cracking and hydrogen embrittlement susceptibility of an eutectoid steel employed in prestressed concrete. *Corrosion Science, 45*(9), 1969-83.

Wang X, Liu X. (2004). Bond strength modeling for corroded reinforcements in reinforced concrete. *Structural Engineering and Mechanics, 17*(6), 863-78.

Zhang B BB. (2004). Design and evaluation of a new bond-type anchorage system for fiber reinforced polymer tendons. *Can J Civ Eng, 31*(1),

Zhang HY, Kodur V, Wu B, Yan J, Yuan ZS. (2018). Effect of temperature on bond characteristics of geopolymer concrete. *Construction and Building Materials,163*, 277-85.

Zhi Fang KZ, Bing Tu. (2013). Experimental investigation of a bond-type anchorage system for multiple FRP tendons. *Engineering Structures, 57*, 364-73.